PtdIns(3,4)P_2, Lamellipodin, and VASP coordinate cytoskeletal remodeling during phagocytic cup formation in macrophages.

Fernando Montaño-Rendón[1,2], Glenn F. W. Walpole[1,3], Matthias Krause[4], Gerald R.V. Hammond[5], Sergio Grinstein[1,2,3,6*], Gregory D. Fairn[2,3,6,7*]

[1]Division of Cell Biology, Hospital for Sick Children, Toronto, ON, Canada

[2]Institute of Medical Sciences, University of Toronto, Toronto, ON, Canada

[3]Department of Biochemistry, University of Toronto, Toronto, ON, Canada

[4]Randall Centre for Cell and Molecular Biophysics, King's College London, London, UK

[5]Department of Cell Biology, University of Pittsburgh School of Medicine, Pittsburgh, PA, USA

[6]Keenan Research Centre for Biomedical Science, St. Michael's Hospital, Toronto, ON, Canada

[7]Department of Pathology, Dalhousie University, Halifax, NS, Canada

*e-mail: sergio.grinstein@sickkids.ca; gfairn@dal.ca

Running title: PtdIns(3,4)P_2, Lamellipodin and VASP regulate phagosome formation

Keywords: PI(3,4)P_2, phagocytosis, macrophages, phosphatidylinositol 3-kinase; phosphoinositides, lipid signaling, actin cytoskeleton, fluorescence imaging.

Abstract

Phosphoinositides are pivotal regulators of vesicular traffic and signaling during phagocytosis. Phagosome formation, the initial step of the process, is characterized by local membrane remodelling and reorganization of the actin cytoskeleton that leads to formation of the pseudopods that drive particle engulfment. Using genetically-encoded fluorescent probes we found that upon particle engagement a localized pool of PtdIns(3,4)P_2 is generated by the sequential activities of class I phosphoinositide 3-kinases and phosphoinositide 5-phosphatases. Depletion of the enzymes responsible for this locally generated pool of PtdIns(3,4)P_2 blocks pseudopod progression and ultimately phagocytosis. We show that the PtdIns(3,4)P_2 effector Lamellipodin (Lpd) is recruited to nascent phagosomes by PtdIns(3,4)P_2. Furthermore, we show that silencing of Lpd inhibits phagocytosis and produces aberrant pseudopodia with disorganized actin filaments. Lastly, vasodilator-stimulated phosphoprotein (VASP) was identified as a key actin-regulatory protein mediating phagosome formation downstream of Lpd. Mechanistically, our findings imply that a pathway involving PtdIns(3,4)P_2, Lpd and VASP mediates phagocytosis at the stage of particle engulfment.

Introduction

Phagocytosis, the process whereby cells engulf and dispose of effete cells, microorganisms, and foreign particles, is pivotal for immunity and tissue homeostasis[1,2]. Phagosome formation, the initial step during phagocytosis, entails marked reorganization of the actin cytoskeleton and membrane remodelling events that lead to pseudopod extension and particle engulfment[3,4]. Earlier studies have suggested that phosphoinositides are pivotal molecules in the regulation of phagocytosis. Phosphoinositides, which play crucial roles in signaling and membrane traffic[5], reside primarily in the cytosolic leaflet of organelles including the plasma membrane and phagosomes. Phosphatidylinositol 4,5-*bis*phosphate (PtdIns(4,5)P_2) is enriched in the plasma membrane where, amongst its many roles, it acts as a positive regulator of actin polymerization[6]. The conversion of PtdIns(4,5)P_2 to phosphatidylinositol 3,4,5-*tris*phosphate (PtdIns(3,4,5)P_3) is a potent stimulus resulting in alterations in actin dynamics through the activation/inactivation of Rho-GTPases, as well as promoting the hydrolysis of PtdIns(4,5)P_2 by activating phospholipase Cγ. Indeed, it has been appreciated for nearly two decades that IgG-opsonized particle engagement by the phagocytic Fcγ receptor leads to the activation of the phosphoinositide-3-kinase (PI3K)[7] that is required for the internalization of large phagocytic prey[8,9]. Remarkably, the dynamic changes in phosphoinositides and the actin cytoskeleton during phagocytosis are restricted to the site of particle engagement and do not propagate to the rest of the plasma membrane. Accordingly, phagosome formation is characterized by the focal generation of PtdIns(3,4,5)P_3[10] at the site of contact and extending pseudopods, while a concomitant disappearance of PtdIns(4,5)P_2 is observed at the base of the phagocytic cup prior to sealing of the nascent phagosome[11].

The downstream effects of PI3K activation during phagocytosis have been mostly attributed to the generation of PtdIns(3,4,5)P_3. However, some of these findings should be interpreted with caution, as most were obtained using probes with dual specificity for PtdIns(3,4,5)P_3 and PtdIns(3,4)P_2, such as the pleckstrin-homology (PH) domain of Akt[12,13]. Recent advances in lipid bio-sensor design have enabled the distinction of the differential roles of PtdIns(3,4,5)P_3 and the related PtdIns(3,4)P_2[14,15]. PtdIns(3,4)P_2 is increasingly appreciated as involved in cellular processes such as endocytosis, cell migration, and neurite initiation[16,17,18,19].

To date, however, the role of PtdIns(3,4)P_2 and its effectors during phagocytosis remains largely unknown. Using recently developed specific probes we demonstrate here that PtdIns(3,4)P_2 accumulates greatly at sites of phagocytosis, where it persists long after PtdIns(3,4,5)P_3 disappears. More importantly, we show that selective depletion of PtdIns(3,4)P_2 attenuates particle internalization, highlighting the importance of this unique phosphoinositide.

Results

Detection of PtdIns(3,4)P_2 in the plasma membrane of resting macrophages

The distribution of PtdIns(3,4)P_2 in unstimulated RAW 264.7 macrophages was investigated first. To this end we employed a recently described genetically-encoded biosensor based on tandem carboxy-terminal PH (cPH) domains of TAPP1[20,21] . Using these biosensors, NES-mCh-cPHx3 and NES-EGFP-cPHx2 (cPHx3 and cPHx2 respectively), we detected a discrete plasmalemmal pool of PtdIns(3,4)P_2 in resting cells (Figure 1A, left panel). To confirm the specificity and responsiveness of the probes we co-expressed inositol polyphosphate 4-phosphatase type II (INPP4B), which selectively hydrolyzes the D-4 position of PtdIns(3,4)P_2 [22,23]. To ensure plasmalemmal targeting of INPP4B, the phosphatase was attached to a carboxy-terminal CAAX motif (INPP4B-CAAX) that is prenylated and polycationic. As shown in Figure 1A (middle and right panels) the biosensors detached from the membrane upon co-expression of INPP4B-CAAX, but not when the catalytically inactive INPP4B(C842A)-CAAX mutant was co-expressed. These observations validate the selectivity of the probes and confirm that modest yet detectable amounts of PtdIns(3,4)P_2 are indeed present in the membrane of resting macrophages. Furthermore, we documented that production of PtdIns(3,4)P_2 is PI3K-dependent, since treatment with nanomolar concentrations of the PI3K inhibitor wortmannin completely released the cPHx3 probe from the plasma membrane (Figure 1B,C).

PtdIns(3,4)P_2 accumulates at the site of particle engagement during phagocytosis

Next, we examined the distribution of PtdIns(3,4)P_2 during phagocytosis. Upon exposure to IgG-opsonized sheep erythrocytes (SRBCs), RAW 264.7 cells exhibited a marked accumulation of the PtdIns(3,4)P_2 probe at the site of phagocytosis to levels greatly surpassing those of the neighbouring unengaged plasma membrane, an observation consistent with stimulated local production of the lipid (Figure 2A, left panel). PtdIns(3,4)P_2 accumulated in the phagosomal cup and remained in the membrane even after scission of the nascent phagosome (Video S1.). Of note, there were marked differences in the distribution and dynamics of recruitment of cPHx2 and PH-BTKx2 (a sensor for PtdIns(3,4,5)P_3) during phagocytosis. Specifically, PtdIns(3,4,5)P_3 accumulated primarily – albeit transiently – at the base of the phagocytic cup, whereas

PtdIns(3,4,)P_2 was acquired slightly later, initially attaining higher levels at the tips of the extending pseudopods (Figure S1., Video S2.) and later persisting for a few minutes in the sealed phagosome. The accumulation of the PtdIns(3,4)P_2 probe at the phagosomal cup was largely obliterated by co-expression of the INPP4B-CAAX construct, but no depletion was observed when the catalytically-inactive INPP4B(C842A)-CAAX construct was used as negative control (Figure 2A and B). These findings imply that PtdIns(3,4)P_2 is produced locally at sites of phagocytosis.

Phagosomal PtdIns(3,4)P_2 is produced downstream of Class I PI3K and 5-phosphatases

We next sought to elucidate the pathway(s) responsible for the biosynthesis of PtdIns(3,4)P_2 during phagocytosis. We considered two possibilities, which are not mutually exclusive: that the PtdIns(3,4)P_2 was being produced by dephosphorylation of PtdIns(3,4,5)P_3 and/or that it was synthesized from PI(4)P by class II PI3Ks. Class I PI3K is known to be activated during phagocytosis and its inhibition arrests engulfment by preventing full extension of the pseudopods around the particle[8,9]. To assess its involvement, we treated cells with nanomolar concentrations of the pan-PI3K inhibitor PI-103 or the class I PI3K-selective inhibitor GDC-0941 and monitored PtdIns(3,4)P_2 formation during phagocytosis (Figure 2C and D). In both cases the recruitment of cPHx2 was virtually eliminated, consistent with a major role for class I PI3Ks in the generation of PtdIns(3,4)P_2. Nevertheless, we examined the possible contribution of Class II PI3Ks. For this, we acutely depleted the plasmalemmal pool of PtdIns(4)P using GSK-A1, a potent and specific inhibitor of the type III phosphatidylinositol 4-kinase PI4KA (PI4KIIIα) that is largely responsible for the generation and maintenance of plasmalemmal PtdIns(4)P; it is noteworthy that selective inhibition of PI4KIIIα by GSK-A1 does not acutely alter the plasmalemmal levels PtdIns(4,5)P_2[24], the substrate of class I PI3Ks. Upon treatment with GSK-A1, the recruitment of mCherry-cPHx3 to the phagocytic cup remained largely unaffected despite a profound depletion of PtdIns(4)P monitored by the high-avidity biosensor 2xP4M (Figure 2E). These findings strongly suggest that dephosphorylation of PtdIns(3,4,5)P_3 is the main source of PtdIns(3,4)P_2 production at the phagocytic cup.

The involvement of PI3Ks that generate PtdIns(3,4,5)P_3 suggests that phosphoinositide 5-phosphatases are also required for the synthesis of PtdIns(3,4)P_2 during phagocytosis. Multiple 5-phosphatases could in theory play a role in the production of PtdIns(3,4)P_2. For instance, Src homology 2 (SH2) domain-containing inositol-5-phosphatase 2 (SHIP2) is involved in the production of PtdIns(3,4)P_2 at sites of endocytosis[25] and at invadopodia[26]. Importantly, SHIP2 has also been reported to translocate to sites of phagocytosis[27], making it an attractive candidate to mediate the production of PtdIns(3,4)P_2. However, overexpression of the catalytically-inactive mutant of SHIP2 (D607A), which is expected to exert a dominant-negative effect, had no effect over phagosomal levels of PtdIns(3,4)P_2 (Figure S2 A and B). Similar negative results were observed when the cells were treated with either a SHIP2-selective inhibitor (AS1949490) or with the pan-SHIP1/2 inhibitor (K118) (Figure S2 C). We therefore turned our attention to other 5-phosphatases: there is compelling evidence that SHIP1[28], INPP5E[29], and OCRL[30] are all recruited to nascent phagosomes. In addition, we identified synaptojanin-2 (SYNJ2) and INPP5B as being present at the site of phagocytosis (Figure 2F). It is therefore conceivable that multiple 5-phosphatases collaborate to dephosphorylate PtdIns(3,4,5)P_3 to PtdIns(3,4,)P_2[1]. Because of the likelihood of functional redundance, the identity of the specific phosphatases involved was not pursued further.

Depletion of PtdIns(3,4)P_2 impairs phagosome formation

We next sought to determine whether PtdIns(3,4)P_2 accumulation is necessary for efficient FcγR-mediated particle uptake. To this end, phagocytic efficiency was compared in RAW 264.7 macrophages over-expressing INPP4B-CAAX to deplete plasmalemmal PtdIns(3,4)P_2, or the catalytically inactive version INPP4B(C842A)-CAAX, used as a negative control. We observed a stark decrease in the phagocytic efficiency of cells expressing the INPP4B-CAAX, compared to cells expressing the INPP4B(C842A)-CAAX mutant (Figure 3A,B). Since particle binding seemed unaffected by INPP4B-CAAX expression (Figure 3A, right panel), we hypothesised that a defect in pseudopod extension or sealing must be responsible for the observed decrease in phagocytic efficiency.

Actin remodelling, which drives pseudopod extension, is a hallmark of the early stages of the phagocytic process. To assess the role of PtdIns(3,4)P_2 in actin polymerization we performed live-cell imaging of cells co-expressing LifeAct-GFP and either INPP4B-CAAX or INPP4B(C842A)-CAAX. In cells expressing the inactive phosphatase, focal actin polymerization was followed by pseudopod formation, and progressive particle engulfment in a zipper-like fashion (Figure 3C, right; Fig. 3D, bottom row and Video S2.). In contrast, cells where PtdIns(3,4)P_2 was depleted by expression of INPP4B-CAAX, formed pseudopods that failed to progress and wrap around the phagocytic target, despite exhibiting an apparently normal initial actin polymerization (Figure 3C left; Fig. 3D, top row, and Video S3.). These findings indicate that PtdIns(3,4)P_2 is necessary for phagocytosis and that it plays a direct role in regulating actin organization and pseudopod progression during the early stages of particle engulfment.

Lamellipodin, a PtdIns(3,4)P_2 effector, accumulates at the phagocytic cup

To date, only a handful of proteins have been identified as specific effectors of PtdIns(3,4)P_2[18]. These include the modular adaptor protein Ras-associated and pleckstrin homology domains-containing protein 1, more commonly referred to as Lamellipodin (Lpd). Through its ability to cluster and tether Ena/VASP proteins to actin filaments, Lpd is a key regulator of the actin cytoskeleton[32]. As such Lpd has roles in lamellipodial formation[33], stabilization of actin-dependent cellular protrusions[34], cell migration and endocytosis[25,35–38]. Because the PH domain of Lpd has been shown to bind PtdIns(3,4)P_2[33], it appeared a likely candidate for the regulation of pseudopod extension during particle engulfment. To examine this possibility, Lpd was expressed in RAW 264.7 macrophages and its distribution assessed during phagocytosis of IgG-opsonized SRBCs. We observed robust accumulation of GFP-Lpd at the phagocytic cup, where PtdIns(3,4)P_2 was also enriched (Figure 4A). Furthermore, upon treatment with wortmannin the levels of both PtdIns(3,4)P_2 and Lpd at the phagocytic cup decreased in parallel fashion (Figure 4B,C). Consistent with the notion that Lpd binds to PtdIns(3,4)P_2 via its PH domain, we found that a GFP-tagged tandem PH domain of Lpd (Lpd-2xPH) was recruited to the phagocytic cup in cells expressing the inactive INPP4B(C842A)-CAAX (Figure 4D) yet failed to accumulate in cells expressing INPP4B-CAAX. Furthermore, in resting

RAW 264.7 cells, Lpd-2xPH showed modest accumulation at the plasma membrane, as we had seen earlier for the cPHx3 and cPHx2 probes, and this limited recruitment was similarly abolished by INPP4B-CAAX, but not by the catalytically-inactive INPP4B(C842A)-CAAX (Figure S3). From these experiments we conclude that Lpd is recruited early during phagocytosis at least in part by its PH domain-mediated interaction with PtdIns(3,4)P_2.

Silencing of Lpd results in aberrant phagocytic cups and arrests phagocytosis

We next sought to determine whether Lpd is necessary for FcγR-mediated phagocytosis. The expression of endogenous Lpd in RAW 264.7 macrophages and its susceptibility to shRNA-mediated silencing were first validated by immunostaining (Figure 5A). The enrichment of the endogenous Lpd during phagocytosis was similarly confirmed by immunostaining; its distribution at the phagocytic cup closely resembled that of F-actin stained with phalloidin (Figure 5B). Upon silencing of Lpd, we observed an aberrant "flaring" of F-actin around the opsonized particle (Figure 5C, top right panel). Lpd-silenced macrophages exhibited "loose" phagocytic cups characterized by multiple protrusions, in contrast to the tightly apposed pseudopods of control cells. In addition, Lpd-shRNA cells exhibited a ~60% decrease in phagocytic efficiency compared to control cells (Figure 5D, E). Taken together, these findings suggest that Lpd is necessary for proper F-actin organization and pseudopod extension during phagocytosis.

The Lamellipodin ligand VASP localizes to the phagocytic cup and is necessary for phagocytosis

Ena/VASP proteins promote actin polymerization by accelerating filament elongation and opposing the action of capping proteins[39–41]. Ena/VASP proteins regulate the cytoskeleton during T cell receptor (TCR)-signalling[42] and also play a role in Fc-mediated phagocytosis[43]. It is relevant that Ena/VASP proteins harbour an EVH1 domain that interacts with the multiple proline-rich regions (FPPPP) present in Lpd[32,33] (Figure 6A) and that they jointly regulate the dynamics of filopodia[44]. We sought to determine if Lpd and VASP associate within the phagocytic cup. Co-expression of the Lpd and VASP constructs revealed colocalization of these

proteins during phagocytosis. Notably, Lpd, VASP and F-actin all share a similar distribution within the phagocytic cup (Figure 6B).

Next, we tested whether VASP was necessary for phagocytosis. To this end, we took advantage of the *Listeria monocytogenes* effector protein ActA which binds tightly to VASP. We expressed an N-terminally truncated ActA protein which includes the four repeats of the VASP-binding sequences attached to a C-terminal motif that targets the protein to the cytosolic surface of mitochondria (mRFP-Mito-FP4)[45,46]. Expression of mRFP-Mito-FP4 effectively sequestered the vast majority of VASP to the mitochondria and prevented its accumulation at the phagocytic cup, while a mutant version (mRFP-Mito-AP4) that also targets to mitochondria but is unable to bind VASP was without effect (Figure 6C). Tethering of VASP to the mitochondria by means of mRFP-Mito-FP4 reduced the phagocytic efficiency from 79.8% to 31.4% (Figure 6D). These results demonstrate that VASP is a positive regulator of phagocytosis and support the notion that Lpd is exerting its effects at least in part by binding to VASP.

Lamellipodin-VASP interactions coordinate actin polymerization at the phagocytic cup

Next, we examined whether the interaction between Lpd and VASP was necessary for phagocytosis. We overexpressed a mutant version of Lpd in which all Ena/VASP-binding sites had been inactivated through mutations (Lpd^{EVmut}). Overexpression of GFP-Lpd^{EVmut} produced a ~57% decrease in phagocytosis when compared to RAW 264.7 cells transfected with the wild-type GFP-Lpd construct (Figure 7A-B). Furthermore, even though the initial recruitment of GFP-Lpd^{EVmut} to the phagocytic cup was unaffected, the distribution of the construct became altered during phagocytic cup formation (Figure S4.). We noticed that the phagocytic cups formed by this mutant contained multiple filopodia- and ruffle-like projections that were rich in F-actin, as visualized through phalloidin staining (Figure 7C). These atypical phagocytic cups and pseudopods closely resembled the ones we had previously observed upon silencing of Lpd (Figure 5C). Additionally, these aberrant phagocytic cups were also enriched in PtdIns(3,4)P_2, detected by the cPHx3 probe (Figure 7D) demonstrating that the lipid metabolism itself was unperturbed by expression of the Lpd mutant. These findings suggest that interactions between

Lpd and VASP are required for proper cytoskeleton organization and coordinated extension of pseudopods at the site of particle engulfment.

Discussion

We found that comparatively small amounts of PtdIns(3,4)P_2 are present in the plasma membrane of resting RAW 264.7 macrophages and that this phosphoinositide is greatly enriched at the sites of particle engagement during FcγR-mediated phagosome formation. Selective depletion using a highly specific phosphatase revealed that PtdIns(3,4)P_2 has a critical role in supporting phagocytosis. This was previously unrecognized in part due to the use of probes like AKT-PH that have dual specificity and of PI3K inhibitors, rather than targeted enzymatic depletion by INPP4B. We also report that Lpd and its binding partner VASP are jointly required for robust phagocytosis: loss of either from the site of phagocytosis results in an atypical and seemingly uncoordinated actin assembly within the extending pseudopods that hence fail to encircle the target.

The importance of PI3Ks during the process of phagocytosis has been widely documented[47,48,49]. Genetic manipulation of PI3Ks as well as the use of pharmacological inhibitors impairs phagocytosis, particularly that of larger targets. Although some of these defects can be directly linked to the role of PtdIns(3,4,5)P_3 cognate effectors, based on this study it is likely that a second, underappreciated effect of PI3K inhibition is the impairment of PtdIns(3,4)P_2 formation, which is itself required for phagocytosis. Curiously, in our studies we find that PtdIns(3,4)P_2 is found at both the base of the phagocytic cup as well as at the tips of the pseudopods, whereas PtdIns(3,4,5)P_3 is largely restricted to the base of the phagocytic cup (Figure S1). This raises the possibility that the relevant phosphoinositide 5-phosphatases are particularly active at the tips of the advancing pseudopods. Phenotypically, inhibition of PI3K – and thus attenuation of both PtdIns(3,4)P_2 and PtdIns(3,4,5)P_3 production– results in arrest of pseudopod progression roughly halfway around the opsonized particle[9,50], while selective depletion of PtdIns(3,4)P_2 prevents pseudopod extension (Figure 3C right panel, 3D, and Video S3). PtdIns(3,4,5)P_3 is thought to regulate actin dynamics during phagocytosis by locally activating Rho family GEFs and GAPs[51], and by activating phospholipase Cγ, thereby depleting

PtdIns(4,5)P_2 from the base of the phagocytic cup. In view of our observations, it seems worthwhile to reconsider whether the purported PtdIns(3,4,5)P_3 effectors are in fact selective for this lipid or are instead responsive to PtdIns(3,4)P_2.

An earlier report suggested that the inositol polyphosphate 4-phosphatase type 1 (INPP4A), which is expressed in RAW macrophages, is a negative regulator of phagocytosis[52]. That study documented enhanced ability to internalize particles by RAW cells expressing shINPP4A and by primary macrophages from *INPP4A*-knockout mice. While the authors did not provide a mechanistic explanation for the observed effects, their findings are consistent with our conclusion that increased PtdIns(3,4)P_2 is essential for optimal phagocytosis, at least partly via Lpd and VASP.

Lpd belongs to the Mig-10, RIAM, Lpd (MRL) family of modular adaptor proteins[53]. RIAM, despite sharing homology with Lpd[54], is thought to act downstream of Rap1, and evidence suggests that its PH domain binds preferentially to PtdIns(3)P, PtdIns(5)P [55] and PtdIns(4,5)P_2[56,57], not PtdIns(3,4)P_2. Previously, RIAM was described to support complement-dependent phagocytosis by relaying integrin signaling[58]. However, RIAM is not required for FcγR-dependent phagocytosis[59], the mode we studied. Furthermore, our results indicate that silencing of Lpd produces severe defects in the phagocytic cups of macrophages where RIAM was left intact. These findings suggest that Lpd, contrary to RIAM, is necessary for Fc-mediated phagocytosis and that these MRL proteins play non-redundant roles during this process.

We found that the PH domain of Lpd is sufficient for its localization at the phagocytic cup. It is possible however, that other interactions contribute to its recruitment and retention within the forming phagosome. Indeed, we noted that Lpd dissociates from the maturing phagosome prior to the disappearance of the PtdIns(3,4)P_2, suggesting that it may function as a co-incidence detector; other potential binding partners may well be present at the site of phagocytosis. In this regard, it is noteworthy that Lpd directly binds actin filaments through an unstructured and highly basic region in its carboxyl-terminus[32]. Furthermore, Lpd can also bind to active Rac1[60,61], which is similarly recruited to forming phagocytic cups[62]. Additionally, the formin-binding protein 17 (FBP17) binds to Lpd and recruits it to the membrane during fast

endophilin-mediated endocytosis[63]. Of note, FPB17 is also present within podosomes and phagocytic cups in macrophages[64].

Lpd is central to the regulation of cytoskeletal dynamics[33] as it interacts with multiple actin regulators such as the Ena/VASP family proteins[32,36,65] and the SCAR/WAVE regulatory complex[36,60]. Ena/VASP proteins localize to the phagocytic cup and are indispensable for phagocytosis: Coppolino *et al.*[43] reported that upon binding of Ena/VASP to a cytosolic GFP-ActA construct, phagocytosis was inhibited. In the current study, we were able to validate these findings using a more thorough method that entailed mistargeting Ena/VASP proteins to the mitochondria. Additionally, we found that all three Ena/VASP family members (EVL, Mena, VASP) localize to the phagocytic cup when ectopically expressed (Figure S5.). Phosphorylation of Lpd by c-Abl kinase reportedly increases its interaction with Ena/VASP [66]. While we did not explore this possibility in the current study, Abl family kinases have been implicated in the positive regulation of phagocytosis[67]. Therefore, it is possible that a kinase-dependent increase in Lpd – Ena/VASP interaction is one of the mechanisms by which this positive regulation takes place. Furthermore, PI3K activation through Abl kinase was also recently reported to take place during podosome formation in macrophages[68].

In addition to VASP, Lpd can also regulate the actin cytoskeleton through its interactions with the SCAR/WAVE complex. A recent study demonstrated that loss of the WAVE regulatory complex (WRC) impairs phagocytosis[69]. In our study, we compared the effects of Lpd mutants in which all Ena/VASP or all SCAR/WAVE binding sites had been mutated. The Lpd^{EVmut} caused the most robust decrease in phagocytic efficiency and aberrant phagocytic cups (Figure 7). Nevertheless, the SCAR/WAVE binding-deficient mutant also exhibited a smaller, yet significant, decrease in phagocytic efficiency (Figure S6). Furthermore, Abi1, the component of the WRC which interacts directly with Lamellipodin[60], was also localized to the phagocytic cup (Figure S6). Jointly, these findings suggest that Lpd is central to the regulation of actin dynamics during phagocytic cup formation not only through its interactions with VASP, but probably also through the regulation of the WRC, although additional experiments will be needed to validate the involvement of the latter pathway.

Methods

Plasmids

The plasmids used in this study are summarized in Table 1. Where indicated, plasmids were constructed using In-Fusion HD EcoDry Cloning Kits (Takara 121416) and were verified by Sanger sequencing prior to transfection into mammalian cells.

Cell Culture

The murine macrophage RAW 264.7 cell line was obtained from the American Type Culture Collection (Manassas, VA) and cultured in DMEM (Wisent Bioproducts, Saint-Jean-Baptiste, Canada) supplemented with 10% heat-inactivated fetal bovine serum and incubated at 37°C under 5% CO_2.

Phagocytosis assays

Quantitative phagocytosis assays have been described previously[70]. Briefly, ~5×10^4 cells were seeded onto 1.8-cm glass coverslips and grown for 18–24 h. Opsonization of SRBC was performed by incubating 100 µL of a 10% SRBC suspension with 3 µL of rabbit IgG fraction against SRBCs at 37°C for 1 h. SRBCs were then labelled with a fluorescent secondary antibody against rabbit. 10 µL of labelled and opsonized SRBCs was added to individual coverslips containing RAW cells within 12-well plates or directly into imaging chambers for live-cell imaging. Synchronization of phagocytosis was achieved by centrifugation (300 ×*g* for 10 s) of the phagocytic targets onto the cell-containing coverslips.

Antibodies and reagents

Rabbit polyclonal Lpd antibody[33] was used for immunofluorescence at 1:200. SRBCs 10% suspension was purchased from MP Biomedicals (Santa Ana, CA). Anti-sheep red blood cell antibodies were purchased from Cedarlane Laboratories (Burlington, Canada). Fluorescent secondary antibodies against mouse and rabbit were purchased from Jackson ImmunoResearch Labs (West Grove, PA). Paraformaldehyde (16% w/v) was purchased from Electron Microscopy Sciences (Hatfield, PA). Wortmannin (Sigma 681675), PI-103 (Sigma 528100), GDC-0941

(Millipore Sigma 509226), GSK-A1 (kindly provided by Dr. Tamas Balla[24]), AS1949490 and K118 (Echelon Biosciences). Fluorescent phalloidin (Molecular Probes). Phosphate-buffered saline (PBS) and Hanks' balanced salt solution (HBSS) (Wisent Bioproducts, Saint-Jean-Baptiste, Canada.

Transfections

RAW 264.7 cells were plated in 18 mm round coverslips ~36–40 h before experiments. Subsequently, cells were transfected using Fugene HD (Promega) according to the manufacturer's protocol. Briefly, 1 µg of plasmid DNA was mixed with 3 µL of Fugene HD in 100 µL of serum-free DMEM. The mix was incubated for 15 min at room temperature, then distributed into two wells of a 12-well plate containing cells seeded onto glass coverslips. Experiments were performed ~16–18 h post-transfection.

Inducible cell line generation

Transgenic, doxycycline-inducible RAW 264.7 stable lines were generated by the Sleeping Beauty transposon system[71]. The open reading frames of TagBFP2-INPP4B(WT)-CAAX or TagBFP2-INPP4B(C842A)-CAAX were inserted into the pSBTet-pur backbone. pSBTet-pur plasmids were co-transfected in a 10:1 ratio to pCMV(CAT)-T7-SB100 in 6-well plates using FuGENE HD as described above. Cell culture medium was replaced 18 hours later and, to select for genomic integration, RAW 264.7 cells were incubated with 2.5 µg/mL puromycin (Sigma P8833). Puromycin selection was maintained for 5 days prior to expanding the polyclonal population into culture flasks for expansion and validation. For induction of TagBFP2-fusions, 1 µg/mL doxycycline (Hyclate, Sigma D9891) was added to the culture medium for 48 hours. Generally, ~50% of the polyclonal RAW 264.7 cell population exhibited robust expression of the transgenes.

Immunostaining

Paraformaldehyde (4% w/v)-fixed cells were permeabilized in 0.1 % (v/v) Triton X-100 in PBS for 7 min, blocked in 2% (w/v) BSA in PBS for 1 hour at room temperature or overnight at 4°C.

Then, coverslips were incubated for 1 hour with primary antibodies (diluted in 2% BSA), washed multiple times in PBS and subsequently incubated with secondary antibodies (diluted in PBS) for 1 hour.

Confocal microscopy and image processing

Confocal fluorescence microscopy was performed using spinning-disk confocal microscopes (Quorum Technologies). Our systems use an Axiovert 200M microscope (Carl Zeiss) equipped with a ×63 oil immersion objective (NA 1.4) and a ×1.5 magnifying lens. These microscopes carry a motorized XY stage (Applied Scientific Instrumentation), a piezo Z-focus drive and diode-pumped solid-state lasers emitting at 440, 491, 561, 638 and 655 nm (Spectral Applied Research). Images were recorded with back-thinned, cooled charge-coupled device cameras (Hamamatsu Photonics). Acquisition settings and capture are controlled by Volocity software v6.2.1 (PerkinElmer). Selection of regions of interest, fluorescence intensity measurements and brightness–contrast corrections were performed with Volocity software or with FIJI (National Institutes of Health). Brightness and contrast parameters were adjusted across entire images without altering the linearity of mapped pixel values. For live-cell imaging, cells grown on glass coverslips were mounted in a Chamlide magnetic chamber (Seoul, South Korea), filled with 1 mL of HBSS and kept at 37°C with a heating stage.

Statistics and reproducibility

Statistical analyses were performed using GraphPad PRISM. Statistical details for each experiment are also stated in the figure legends. Statistical significance (****$P < 0.0001$, ***$P < 0.001$, **$P < 0.01$, *$P < 0.05$ and NS (not significant)) is denoted in figures when applicable. All microscopy-based experiments were performed independently at least three times.

Table 1.

Plasmid	Backbone vector	Reference
NES-EGFP-cPHx2	pNES-EGFP-C1	21
NES-EGFP-cPHx3	pNES-EGFP-C1	21
NES-mCherry-cPHx3	pNES-mCherry-C1	21
NES-mCherry-PH-BTKx2	pNES-mCherry-C1	Walpole et al., Nature Cell Biology 2022
EGFP-P4Mx2	pEGFP-C1	72
mCherry-P4Mx2	mCherry-C1	72
TagBFP2-INPP4B^{WT}-CAAX	pTagBFP2-C1	21
TagBFP2-INPP4B^{C842A}-CAAX	pTagBFP2-C1	21
pSBtet-pur-TagBFP2-INPP4B(WT)-CAAX	pTagBFP2-C1	This study
pSBtet-pur-TagBFP2-INPP4B(C842A)-CAAX	pTagBFP2-C1	This study
pSBtet-pur		PMID: 25650551; Addgene #60507
pSBtet-BP		PMID: 25650551; Addgene #60496
pCMV(CAT)-T7-SB100		PMID: 19412179; Addgene #34879
NES-mCherry-PH-BTKx2		This study
GFP-Lpd^{EVmut}	pEGFP-C1	60
GFP-Lpd$^{S/Wmut}$	pEGFP-C1	60
GFP-Lpd	pEGFP-C1	33
Lifeact-EGFP	pEGFP-C1	PMID: 26317264; Addgene #58470
GFP-Lpd(2xPH)	pEGFP-C1	33
GFP-Lpd(ΔPH)	pEGFP-C1	73
mRFP-Mito-FP4	mRFP	74
mRFP-Mito-AP4	mRFP	74
pmScarlet-EVL	pmScarlett	Gift from M. Krause (King's College London)
pmScarlet-VASP	pmScarlett	Gift from M. Krause (King's College London)

pmScarlet-Mena	pmScarlett	Gift from M. Krause (King's College London)
mCitrine-VASP-5	mCitrine	Addgene #56571
mCherry-VASP-5	mCherry	Addgene #55151
shRNA mouse Lpd	pLL3.7-Puro	33
pEGFP-C2-SHIP2 D607A	pEGFPC2	MRCPPU Reagents, University of Dundee
GFP-SHIP2	pEGFPC2	MRCPPU Reagents, University of Dundee
Inpp5B-GFP	pEGFP-C1	75
pEGFP-Abi1	pEGFP-C1	Addgene #74905

Figure Legends

Figure 1. PtdIns(3,4)P_2 at the plasma membrane of RAW 264.7 macrophages.

(A) Confocal section of RAW 264.7 macrophages expressing GFP-cPHx2 alone (left) or in combination with either BFP-INPP4B-CAAX (middle) or BFP-INPP4B(C842A)-CAAX (right); insets represent the BFP. (B) Representative confocal micrographs of RAW 264.7 cells expressing mCherry-cPHx3 in either control (top) or 100 nM wortmannin-treated (bottom) conditions. (C) Normalized plasmalemmal mCherry-cPHx3 fluorescence intensity in control and wortmannin-treated cells. For quantitation, plasmalemmal fluorescence intensity was normalized to cytosolic fluorescence intensity. Unpaired *t*-test of individual values across n=3 independent experiments.

Figure 2. PtdIns(3,4)P_2 accumulates at the site of particle engagement during phagocytosis, is susceptible to the degradation by INPP4B phosphatases, and its production is downstream of class I PI3Ks and 5' phosphatases.

(A) Confocal sections of RAW 264.7 macrophages expressing GFP-cPHx2 alone (left) or in combination with either BFP-INPP4B-CAAX (grey inset) (middle) or BFP-INPP4B(C842A)-CAAX (grey inset) (right) during phagocytosis. Asterisks represent sites of phagocytic cup formation. (B) Normalized phagosomal-cPHx2 fluorescence intensity in INPP4B(C842A)-CAAX and INPP4B-CAAX. For quantitation, here and elsewhere, phagosomal fluorescence intensity was normalized to plasmalemmal fluorescence intensity. Unpaired *t*-test of individual values across n=3 independent experiments, data are mean ± SD. (C) Representative confocal micrographs of RAW 264.7 macrophages expressing GFP-cPHx2 and pretreated with either vehicle control (left), 500 nM PI-103 (middle), or 500 nM GDC-0941 (right). Asterisks denote particles. (D) Normalized phagosomal GFP-cPHx2 fluorescence intensity in control and PI-103-treated cells. Unpaired *t*-test of individual values across n=3 independent experiments, data are mean ± SD. (E) Representative confocal micrographs of RAW 264.7 macrophages co-expressing GFP-2xP4M and mCherry-cPHx3 during phagocytosis in either control (top) or GSK-A1-treated (bottom) conditions. Asterisks indicate sites of particle binding. (F) Representative confocal sections of

RAW 264.7 macrophages expressing SHIP2 (left), SYNJ2 (middle), and INPP5B (right) phosphatases during phagocytosis. Asterisks indicate sites of particle binding.

Figure 3. INPP4B-mediated depletion of PtdIns(3,4)P_2 disrupts phagocytosis.

(A) Representative confocal extended-focus projections of doxycycline-inducible RAW264.7 macrophages expressing BFP-INPP4B(C842A)-CAAX (Control) or BFP-INPP4B-CAAX (PtdIns(3,4)P_2-depleted) following a 10 min incubation with IgG-opsonized SRBCs. Inside-outside staining was performed to differentiate between internalized/total (green) and non-internalized (red) SRBCs. (B) quantification of the phagocytic efficiency in BFP-INPP4B(C842A)-CAAX and BFP-INPP4B-CAAX-expressing RAW 264.7 macrophages. Unpaired *t*-test of individual phagocytic efficiency values of n=228 and 267 cells, respectively across N=3 independent experiments; data are mean ± SEM. (C) Representative live confocal sections of RAW 264.7 macrophages expressing LifeAct-GFP and either BFP-INPP4B(C842A)-CAAX or BFP-INPP4B-CAAX during phagocytosis of IgG-opsonized SRBCs (red). Dotted boxes represent the phagocytic cups tracked in D. (D) Time-lapse microscopy of F-actin dynamics monitored by GFP-Lifeact during phagocytosis of IgG-opsonized SRBCs in RAW 264.7 macrophages expressing BFP-INPP4B-CAAX (top) or BFP-INPP4B(C842A)-CAAX (bottom) (0, 60, 120, and 180 sec timepoints). Scale bar = 3 µm. Similar results were observed in 10 independent experimental repeats.

Figure 4. PtdIns(3,4)P_2 and its effector protein Lamellipodin (Lpd) co-localize at the site of particle engagement during phagocytosis.

(A) Representative confocal sections of RAW 264.7 macrophages co-expressing mCherry-cPHx3 and GFP-Lpd during phagocytosis. Asterisks denote sites of phagocytic cup formation. (B) Representative confocal extended-focus projection of RAW 264.7 macrophages co-expressing mCherry-cPHx3 and GFP-Lpd during phagocytosis following pre-treatment with 100 nM wortmannin. Asterisks represent sites of particle engagement. Inset shows engaged SRBCs (C) Normalized phagosomal Lpd fluorescence intensity in control and wortmannin-treated cells. Unpaired *t*-test of individual values across n=3 independent experiments. (D) Representative confocal micrograph of RAW 264.7 cells co-expressing the tandem PH domain of Lpd (green)

and either BFP-INPP4B(C842A)-CAAX (left) or BFP-INPP4B-CAAX (right) during phagocytosis. Asterisks represent sites of phagocytosis; dotted line delineates the periphery of the cell. Similar results were observed in 5 independent experiments.

Figure 5. Silencing of lamellipodin in macrophages disrupts phagocytosis and yields an aberrant F-actin morphology at the phagocytic cup.

(A) Lpd immunostaining (red) in resting RAW 264.7 macrophages expressing Lpd-shRNA and soluble GFP (green); (B) Lpd immunostaining in control RAW 264.7 macrophages during phagocytosis; (C) Lpd immunostaining in Lpd-silenced RAW 264.7 macrophages (green) during phagocytosis. Asterisks denote sites of particle engagement. Insets are magnifications of the area within the dotted boxes showing Alexa Fluor647-conjugated phalloidin staining (blue) and Lpd staining (red). Similar results were observed in 3 independent experiments. (D) Representative confocal extended-focus projection of RAW 264.7 macrophages with and without expression of Lpd-shRNA (green) following a 10 min incubation with IgG-opsonized SRBCs. Inside-outside staining was performed to differentiate between internalized/total (red) and non-internalized (blue) SRBCs. (E) Quantification of the phagocytic efficiency in Control-shRNA and Lpd-shRNA RAW 264.7 macrophages. Unpaired *t*-test of individual phagocytic efficiency values n=95 (ctrl-shRNA), n=98 (Lpd-shRNA), across N=3 independent experiments; data are means ± SEM.

Figure 6. Lamellipodin and VASP co-localize at the phagocytic cup.

(A) Schematic representation of the functional domains and binding partners of Lpd. Lpd interacts with PtdIns(3,4)P_2 and VASP through its PH domain and FP4 repeats respectively. (B) Representative confocal section of RAW 264.7 macrophages co-expressing Lpd (green) and VASP (red) and stained with phalloidin (blue) during phagocytic cup formation. Similar observations were made in 5 independent experiments. Asterisks indicate sites of particle engagement. (C) Representative confocal slice of RAW 264.7 macrophages co-expressing VASP (green) and either the Mito-AP4 (red, top row) or the Mito-FP4 (red, bottom row) constructs. Similar observations were made in three independent experiments. Asterisks indicate sites of

particle binding. (D) Quantification of the phagocytic efficiency in RAW 264.7 macrophages expressing Mito-AP4 and Mito-FP4 . Unpaired *t* test of individual phagocytic efficiency values n=117 (Mito-AP4), n=127 (Mito-FP4) across N=3 independent experiments; data are means ± SEM.

Figure. 7 Lamellipodin and VASP coordinate actin polymerization at the phagocytic cup. (A) Representative confocal projections of RAW 264.7 macrophages expressing GFP-Lpd (left) and GFP-Lpd^{EVmut} (right) after a 10-min incubation with IgG-opsonized SRBCs. Inside-outside staining was performed to differentiate between internalized/total (red) and non-internalized (blue) SRBCs. (B) Quantification of the phagocytic efficiency in RAW 264.7 macrophages overexpressing either Lpd^{WT} or Lpd^{EVmut}. Unpaired *t* test of individual phagocytic efficiency values n=86 (Lpd^{WT}), n=80 (Lpd^{EVmut}), across N=3 independent experiments; data are means ± SEM. (C) Representative 3D reconstruction of RAW 264.7 macrophages expressing the Lpd^{EVmut} construct (green) during phagocytosis of IgG-opsonized SRBCs and stained with phalloidin (Red) (i) Magnification of the area denoted by the dotted box (i) in main panel, depicting SRBCs (blue). (ii) Magnification of the area denoted by the dotted box (ii) in main panel, depicting a representative phagocytic cup from RAW 264.7 macrophages expressing either the Lpd^{EVmut} (left) or the Lpd^{WT} construct (right) for comparison. Similar observations were made in 3 independent experiments. (D) Representative confocal slice of RAW 264.7 macrophages co-expressing the Lpd^{EVmut} construct (green) and the cPHx3 construct (red) during phagocytosis. Insets represent the area denoted by the dotted box (left) and compared to the Lpd^{WT}-expressing macrophages (right).

References

1. Stuart, L. M. & Ezekowitz, R. A. B. Phagocytosis: elegant complexity. *Immunity* **22**, 539–550 (2005).
2. Flannagan, R. S., Jaumouillé, V. & Grinstein, S. The Cell Biology of Phagocytosis. *Annual Review of Pathology: Mechanisms of Disease* **7**, 61–98 (2012).
3. Levin, R., Grinstein, S. & Canton, J. The life cycle of phagosomes: formation, maturation, and resolution. *Immunological Reviews* **273**, 156–179 (2016).
4. Freeman, S. A. & Grinstein, S. Phagocytosis: Receptors, signal integration, and the cytoskeleton. *Immunological Reviews* **262**, 193–215 (2014).
5. de Craene, J. O., Bertazzi, D. L., Bär, S. & Friant, S. Phosphoinositides, major actors in membrane trafficking and lipid signaling pathways. *International Journal of Molecular Sciences* **18**, (2017).
6. Raucher, D. *et al.* Phosphatidylinositol 4,5-bisphosphate functions as a second messenger that regulates cytoskeleton-plasma membrane adhesion. *Cell* **100**, 221–228 (2000).
7. Gu, H., Botelho, R. J., Yu, M., Grinstein, S. & Neel, B. G. Critical role for scaffolding adapter Gab2 in Fc gamma R-mediated phagocytosis. *The Journal of cell biology* **161**, 1151–61 (2003).
8. Araki, N., Johnson, M. T. & Swanson, J. A. A role for phosphoinositide 3-kinase in the completion of macropinocytosis and phagocytosis by macrophages. *The Journal of Cell Biology* **135**, 1249 LP – 1260 (1996).
9. Cox, D., Tseng, C. C., Bjekic, G. & Greenberg, S. A requirement for phosphatidylinositol 3-kinase in pseudopod extension. *Journal of Biological Chemistry* **274**, 1240–1247 (1999).
10. Dewitt, S., Tian, W. & Hallett, M. B. Localised PtdIns(3,4,5)P3 or PtdIns(3,4)P2 at the phagocytic cup is required for both phagosome closure and Ca2+ signalling in HL60 neutrophils. *Journal of cell science* **119**, 443–451 (2006).
11. Botelho, R. J. *et al.* Localized Biphasic Changes in Phosphatidylinositol-4,5-Bisphosphate at Sites of Phagocytosis. *The Journal of Cell Biology* **151**, 1353 LP – 1368 (2000).
12. Ebner, M., Lučić, I., Leonard, T. A. & Yudushkin, I. PI(3,4,5)P3 Engagement Restricts Akt Activity to Cellular Membranes. *Molecular Cell* **65**, 416-431.e6 (2017).
13. Manna, D., Albanese, A., Park, W. S. & Cho, W. Mechanistic basis of differential cellular responses of phosphatidylinositol 3,4-bisphosphate- and phosphatidylinositol 3,4,5-trisphosphate-binding pleckstrin homology domains. *The Journal of biological chemistry* **282**, 32093–105 (2007).

14. Goulden, B. D. *et al.* A high-avidity biosensor reveals plasma membrane PI(3,4)P₂ is predominantly a class I PI3K signaling product. *The Journal of Cell Biology* **218**, 1066 LP – 1079 (2019).

15. Liu, S.-L. *et al.* Quantitative Lipid Imaging Reveals a New Signaling Function of Phosphatidylinositol-3,4-Bisphophate: Isoform- and Site-Specific Activation of Akt. *Molecular cell* **71**, 1092-1104.e5 (2018).

16. Boucrot, E. *et al.* Endophilin marks and controls a clathrin-independent endocytic pathway. *Nature* **517**, 460–465 (2015).

17. Posor, Y. *et al.* Spatiotemporal control of endocytosis by phosphatidylinositol-3,4- bisphosphate. *Nature* **499**, 233–237 (2013).

18. Li, H. & Marshall, A. J. Phosphatidylinositol (3,4) bisphosphate-specific phosphatases and effector proteins: A distinct branch of PI3K signaling. *Cellular Signalling* **27**, 1789–1798 (2015).

19. Zhang, S. X., Duan, L. H., He, S. J., Zhuang, G. F. & Yu, X. Phosphatidylinositol 3,4-bisphosphate regulates neurite initiation and dendrite morphogenesis via actin aggregation. *Cell Research* **27**, 253–273 (2017).

20. Thomas, C. C., Dowler, S., Deak, M., Alessi, D. R. & van Aalten, D. M. Crystal structure of the phosphatidylinositol 3,4-bisphosphate-binding pleckstrin homology (PH) domain of tandem PH-domain-containing protein 1 (TAPP1): molecular basis of lipid specificity. *The Biochemical journal* **358**, 287–94 (2001).

21. Goulden, B. D. *et al.* A high-avidity biosensor reveals plasma membrane PI(3,4)P2 is predominantly a class I PI3K signaling product. *Journal of Cell Biology* **218**, 1066–1079 (2019).

22. Gewinner, C. *et al.* Evidence that inositol polyphosphate 4-phosphatase type II is a tumor suppressor that inhibits PI3K signaling. *Cancer cell* **16**, 115–125 (2009).

23. Norris, F. A. & Majerus, P. W. Hydrolysis of phosphatidylinositol 3,4-bisphosphate by inositol polyphosphate 4-phosphatase isolated by affinity elution chromatography. *The Journal of biological chemistry* **269**, 8716–8720 (1994).

24. Bojjireddy, N. *et al.* Pharmacological and genetic targeting of the PI4KA enzyme reveals its important role in maintaining plasma membrane phosphatidylinositol 4-phosphate and phosphatidylinositol 4,5-bisphosphate levels. *The Journal of biological chemistry* **289**, 6120–32 (2014).

25. Hak, L. C. W. *et al.* Fbp17 and cip4 recruit ship2 and lamellipodin to prime the plasma membrane for fast endophilin-mediated endocytosis. *Nature Cell Biology* **20**, (2018).

26. Sharma, V. P. *et al.* Tks5 and SHIP2 regulate invadopodium maturation, but not initiation, in breast carcinoma cells. *Current biology: CB* **23**, 2079–2089 (2013).

27. Ai, J. *et al.* The inositol phosphatase SHIP-2 down-regulates FcgammaR-mediated phagocytosis in murine macrophages independently of SHIP-1. *Blood* **107**, 813–820 (2006).

28. Ming-Lum, A. *et al.* A pleckstrin homology-related domain in SHIP1 mediates membrane localization during Fcγ receptor-induced phagocytosis. *FASEB journal: official publication of the Federation of American Societies for Experimental Biology* **26**, 3163–3177 (2012).

29. Segawa, T. *et al.* Inpp5e increases the Rab5 association and phosphatidylinositol 3-phosphate accumulation at the phagosome through an interaction with Rab20. *The Biochemical journal* **464**, 365–375 (2014).

30. Bohdanowicz, M., Balkin, D. M., de Camilli, P. & Grinstein, S. Recruitment of OCRL and Inpp5B to phagosomes by Rab5 and APPL1 depletes phosphoinositides and attenuates Akt signaling. *Molecular biology of the cell* **23**, 176–87 (2012).

31. Malek, M. *et al.* PTEN Regulates PI(3,4)P2 Signaling Downstream of Class I PI3K. *Molecular cell* **68**, 566-580.e10 (2017).

32. Hansen, S. D. & Mullins, R. D. Lamellipodin promotes actin assembly by clustering Ena/VASP proteins and tethering them to actin filaments. *eLife* **4**, 1–29 (2015).

33. Krause, M. *et al.* Lamellipodin, an Ena/VASP ligand, is implicated in the regulation of lamellipodial Dynamics. *Developmental Cell* **7**, 571–583 (2004).

34. Dimchev, G. *et al.* Lamellipodin tunes cell migration by stabilizing protrusions and promoting adhesion formation. *bioRxiv* (2019) doi:10.1101/777326.

35. Dimchev, G. *et al.* Lamellipodin tunes cell migration by stabilizing protrusions and promoting adhesion formation. *Journal of Cell Science* **133**, (2020).

36. Carmona, G. *et al.* Lamellipodin promotes invasive 3D cancer cell migration via regulated interactions with Ena/VASP and SCAR/WAVE. *Oncogene* **35**, 5155–5169 (2016).

37. Lagarrigue, F. *et al.* A RIAM/lamellipodin-talin-integrin complex forms the tip of sticky fingers that guide cell migration. *Nature communications* **6**, 8492 (2015).

38. Vehlow, A. *et al.* Endophilin, Lamellipodin, and Mena cooperate to regulate F-actin-dependent EGF-receptor endocytosis. *The EMBO journal* **32**, 2722–2734 (2013).

39. Barzik, M. *et al.* Ena/VASP proteins enhance actin polymerization in the presence of barbed end capping proteins. *The Journal of biological chemistry* **280**, 28653—28662 (2005).

40. Hansen, S. D. & Mullins, R. D. VASP is a processive actin polymerase that requires monomeric actin for barbed end association. *The Journal of cell biology* **191**, 571–584 (2010).

41. Breitsprecher, D. *et al.* Molecular mechanism of Ena/VASP-mediated actin-filament elongation. *The EMBO journal* **30**, 456–467 (2011).

42. Krause, M. *et al.* Fyn-binding protein (Fyb)/SLP-76-associated protein (SLAP), Ena/vasodilator-stimulated phosphoprotein (VASP) proteins and the Arp2/3 complex link T cell receptor (TCR) signaling to the actin cytoskeleton. *The Journal of cell biology* **149**, 181–194 (2000).

43. Coppolino, M. G. *et al.* Evidence for a molecular complex consisting of Fyb/SLAP, SLP-76, Nck, VASP and WASP that links the actin cytoskeleton to Fcγ receptor signalling during phagocytosis. *Journal of Cell Science* **114**, 4307–4318 (2001).

44. Cheng, K. W. & Mullins, R. D. Initiation and disassembly of filopodia tip complexes containing VASP and lamellipodin. *Molecular biology of the cell* **31**, 2021–2034 (2020).

45. Pistor, S., Chakraborty, T., Niebuhr, K., Domann, E. & Wehland, J. The ActA protein of Listeria monocytogenes acts as a nucleator inducing reorganization of the actin cytoskeleton. *The EMBO journal* **13**, 758–763 (1994).

46. Bear, J. E. *et al.* Negative regulation of fibroblast motility by Ena/VASP proteins. *Cell* **101**, 717–728 (2000).

47. Cox, D. *et al.* Myosin X is a downstream effector of PI(3)K during phagocytosis. *Nature Cell Biology* **4**, 469–477 (2002).

48. Vieira, O. v *et al.* Distinct roles of class I and class III phosphatidylinositol 3-kinases in phagosome formation and maturation. *The Journal of Cell Biology* **155**, 19 LP – 26 (2001).

49. Tamura, N. *et al.* Specific role of phosphoinositide 3-kinase p110alpha in the regulation of phagocytosis and pinocytosis in macrophages. *The Biochemical journal* **423**, 99–108 (2009).

50. Araki, N., Johnson, M. T. & Swanson, J. A. A role for phosphoinositide 3-kinase in the completion of macropinocytosis and phagocytosis by macrophages. *Journal of Cell Biology* **135**, 1249–1260 (1996).

51. Schlam, D. *et al.* Phosphoinositide 3-kinase enables phagocytosis of large particles by terminating actin assembly through Rac/Cdc42 GTPase-activating proteins. *Nature communications* **6**, 8623 (2015).

52. Nigorikawa, K. *et al.* Inositol Polyphosphate-4-Phosphatase Type I Negatively Regulates Phagocytosis via Dephosphorylation of Phagosomal PtdIns(3,4)P2. *PLOS ONE* **10**, e0142091 (2015).

53. Coló, G. P., Lafuente, E. M. & Teixidó, J. The MRL proteins: Adapting cell adhesion, migration and growth. *European Journal of Cell Biology* **91**, 861–868 (2012).

54. Lafuente, E. M. *et al.* RIAM, an Ena/VASP and profilin ligand, interacts with Rap1-GTP and mediates Rap1-induced adhesion. *Developmental Cell* **7**, 585–595 (2004).

55. Jenzora, A., Behrendt, B., Small, J. V., Wehland, J. & Stradal, T. E. B. PREL1 provides a link from Ras signalling to the actin cytoskeleton via Ena/VASP proteins. *FEBS letters* **579**, 455–463 (2005).

56. Patsoukis, N. *et al.* The adaptor molecule RIAM integrates signaling events critical for integrin-mediated control of immune function and cancer progression. *Science signaling* **10**, (2017).

57. Wynne, J. P. *et al.* Rap1-interacting adapter molecule (RIAM) associates with the plasma membrane via a proximity detector. *The Journal of cell biology* **199**, 317–330 (2012).

58. Torres-Gomez, A. *et al.* RIAM-VASP Module Relays Integrin Complement Receptors in Outside-In Signaling Driving Particle Engulfment. *Cells* **9**, 1–18 (2020).

59. Medraño-Fernandez, I. *et al.* RIAM (Rap1-interacting adaptor molecule) regulates complement-dependent phagocytosis. *Cellular and Molecular Life Sciences* **70**, 2395–2410 (2013).

60. Law, A. L. *et al.* Lamellipodin and the Scar/WAVE complex cooperate to promote cell migration in vivo. *Journal of Cell Biology* **203**, 673–689 (2013).

61. Bae, Y. H. *et al.* A FAK-Cas-Rac-lamellipodin signaling module transduces extracellular matrix stiffness into mechanosensitive cell cycling. *Science signaling* **7**, ra57 (2014).

62. Scott, C. C. *et al.* Phosphatidylinositol-4, 5-bisphosphate hydrolysis directs actin remodeling during phagocytosis. *Journal of Cell Biology* **169**, 139–149 (2005).

63. Chan Wah Hak, L. *et al.* FBP17 and CIP4 recruit SHIP2 and lamellipodin to prime the plasma membrane for fast endophilin-mediated endocytosis. *Nature Cell Biology* **20**, (2018).

64. Tsuboi, S. *et al.* FBP17 Mediates a Common Molecular Step in the Formation of Podosomes and Phagocytic Cups in Macrophages. *The Journal of biological chemistry* **284**, 8548–8556 (2009).

65. Chang, Y. C., Zhang, H., Brennan, M. L. & Wu, J. Crystal structure of Lamellipodin implicates diverse functions in actin polymerization and Ras signaling. *Protein and Cell* **4**, 211–219 (2013).

66. Michael, M., Vehlow, A., Navarro, C. & Krause, M. c-Abl, Lamellipodin, and Ena/VASP Proteins Cooperate in Dorsal Ruffling of Fibroblasts and Axonal Morphogenesis. *Current Biology* **20**, 783–791 (2010).

67. Greuber, E. K. & Pendergast, A. M. Abl family kinases regulate FcγR-mediated phagocytosis in murine macrophages. *Journal of immunology (Baltimore, Md.: 1950)* **189**, 5382–5392 (2012).

68. Zhou, Y. *et al.* Abl-mediated PI3K activation regulates macrophage podosome formation. *Journal of cell science* **133**, (2020).

69. Stahnke, S. *et al.* Loss of Hem1 disrupts macrophage function and impacts migration, phagocytosis, and integrin-mediated adhesion. *Current Biology* **31**, 2051-2064.e8 (2021).

70. Montaño, F., Grinstein, S. & Levin, R. Quantitative Phagocytosis Assays in Primary and Cultured Macrophages. *Methods in molecular biology (Clifton, N.J.)* **1784**, 151–163 (2018).

71. Kowarz, E., Löscher, D. & Marschalek, R. Optimized Sleeping Beauty transposons rapidly generate stable transgenic cell lines. *Biotechnology journal* **10**, 647–653 (2015).

72. Hammond, G. R. v, Machner, M. P. & Balla, T. A novel probe for phosphatidylinositol 4-phosphate reveals multiple pools beyond the Golgi. *Journal of Cell Biology* **205**, 113–126 (2014).

73. Boucrot, E. *et al.* Endophilin marks and controls a clathrin-independent endocytic pathway. *Nature* **517**, 460–465 (2015).

74. Bear, J. E. *et al.* Negative regulation of fibroblast motility by Ena/VASP proteins. *Cell* **101**, 717–728 (2000).

75. Erdmann, K. S. *et al.* A role of the Lowe syndrome protein OCRL in early steps of the endocytic pathway. *Developmental cell* **13**, 377–390 (2007).

Supplemental Information

Supplemental Figure 1. PtdIns(3,4)P_2 and PtdIns(3,4,5)P_3 are differentially distributed within the phagocytic cup.

(A) RAW 264.7 macrophages co-expressing the cPHx2 (green) and PH-BTKx2 (magenta) constructs during phagocytic cup formation. (B) Intensity profile from the dotted line in A of the cPHx2 (green) and PH-BTKx2 (magenta) constructs at the phagocytic cup.

Supplemental Figure 2. SHIP1 and SHIP2 are dispensable for PtdIns(3,4)P_2 production at the phagocytic cup.

(A) Representative confocal sections of RAW 264.7 macrophages co-expressing the cPHx3 probe (red) with either the wild-type GFP-SHIP2 (left) or the catalytically-inactive GFP-SHIP2(D607A) (right). (B) Normalized phagosomal-cPHx3 fluorescence intensity in cells co-expressing either wild-type GFP-SHIP2 or the catalytically-inactive GFP-SHIP2(D607A). Unpaired *t* test of individual values across n=3 independent experiments; data are means ± SD. (C) Representative confocal slices of RAW 264.7 macrophages expressing the cPHx2 probe (green) in either control cells (left), or cells pre-treated with the SHIP2 inhibitor AS1949490 10 µM for 5h (middle) or pre-treated with the pan-SHIP1/2 inhibitor K118 5 µM for 5h (right). Asterisks indicate sites of phagocytic cup formation.

Supplemental Figure 3. PtdIns(3,4)P_2 determines the cellular localization of the PH domain of Lpd.

(A) Representative confocal sections of RAW 264.7 macrophages expressing the tandem PH domain of Lpd (green) either alone or in combination with the INPP4B-CAAX construct. Similar results were observed in 3 independent experiments. (B) Representative confocal sections of RAW 264.7 macrophages co-expressing the tandem PH domain of Lpd (green) together with the INPP4B(C842A)-CAAX construct. Similar results were observed in 3 independent experimental repeats.

Supplemental Figure 4. Lpd^{EVmut} during phagocytosis.

(A) Gallery of representative confocal projections of RAW 264.7 expressing the Lpd^{EVmut} construct during phagocytosis. Asterisks denote sites of phagocytic cup formation.

Supplemental Figure 5. EVL, Mena and VASP localize at the phagocytic cup.

(A) Representative confocal sections of RAW 264.7 macrophages stained with phalloidin (green) and expressing VASP (Left), Mena (Middle), and EVL (Right). Insets represent the phagocytic cups denoted by the dotted box. Similar observations were made in 3 independent experimental repeats.

Supplemental Figure 6. Lamellipodin-WRC interactions positively regulate phagocytosis.

(A) Representative confocal slice of a RAW 264.7 macrophage expressing the WRC protein Abi1-GFP during phagocytosis and stained with phalloidin. Insets represent the area denoted by the dotted box. Similar results were obtained in 3 independent experimental repeats. (B) Representative confocal extended-focus projections of RAW 264.7 macrophages expressing Lpd^{SWmut} (left) and $Lpd^{SW/EVmut}$ (right) after a 10-min incubation with IgG-opsonized SRBCs. Inside-outside staining was performed to differentiate between internalized/total (red) and non-internalized (blue) SRBCs. (B) Quantification of the phagocytic efficiency in RAW 264.7 macrophages overexpressing either Lpd^{WT}, Lpd^{EVmut}, Lpd^{SWmut}, and $Lpd^{SW/EVmut}$. One-way ANOVA of individual phagocytic efficiency values n=86 (Lpd), n=80 (Lpd^{EVmut}), n=84 (Lpd^{SWmut}), n=88 ($Lpd^{SW/EVmut}$), across N=3 independent experiments; data are means ± SEM.

Supplemental Video 1. Dynamics of PtdIns(3,4)P_2 and PtdIns(3,4,5)P_3 during phagocytosis

RAW 264.7 macrophages co-expressing the cPHx2(left) and PH-BTKx2 (right) during phagocytosis.

Supplemental Video 2. Actin dynamics during phagocytosis

Actin dynamics in RAW 264.7 macrophages expressing the INPP4B(C842A)-CAAX construct. Similar results were observed in at least 3 independent experiments.

Supplemental Video 3. Actin dynamics in PtdIns(3,4)P_2-depleted macrophages during phagocytosis

Actin dynamics in RAW 264.7 macrophages expressing INPP4B-CAAX construct. Similar results were observed in at least 3 separate experiments.

A

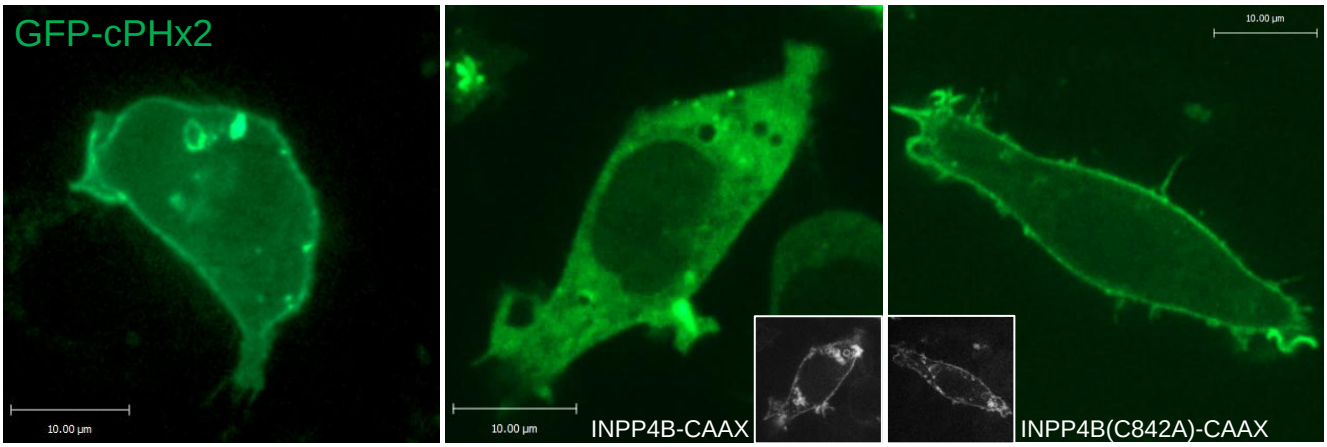
GFP-cPHx2
10.00 µm
10.00 µm
INPP4B-CAAX
10.00 µm
INPP4B(C842A)-CAAX

B

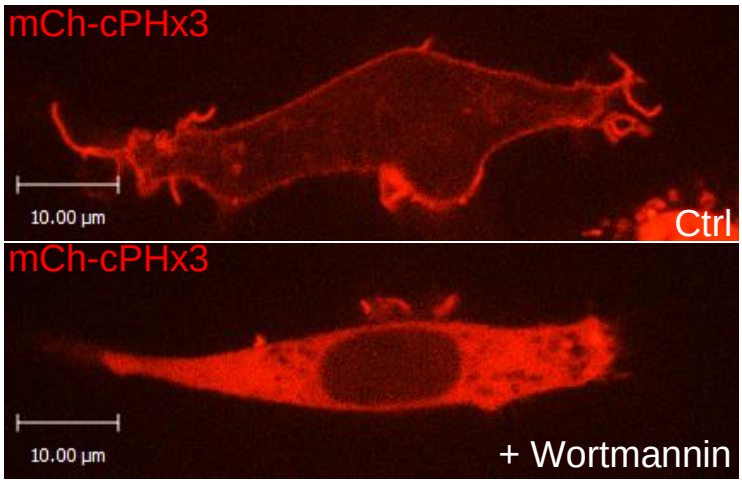
mCh-cPHx3
10.00 µm
Ctrl
mCh-cPHx3
10.00 µm
+ Wortmannin

C

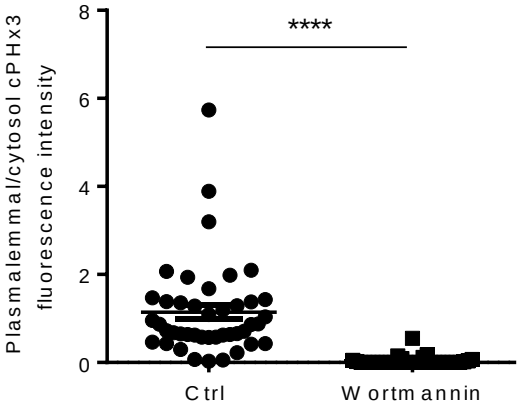
Plasmalemmal/cytosol cPHx3 fluorescence intensity
8
6
4
2
0
****
Ctrl
Wortmannin

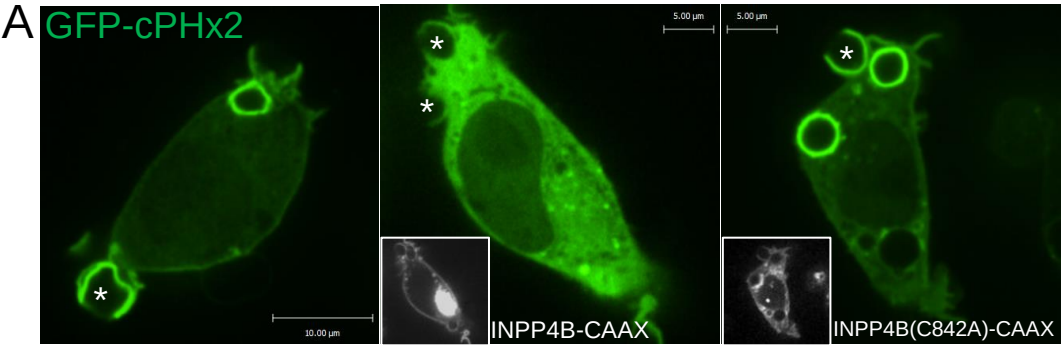
A
GFP-cPHx2
10.00 µm
5.00 µm
INPP4B-CAAX
INPP4B(C842A)-CAAX

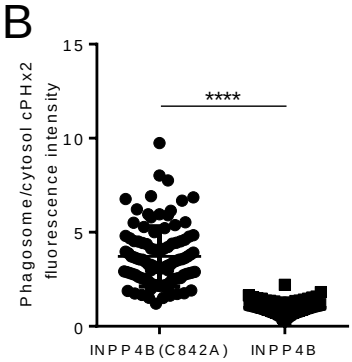
B
Phagosome/cytosol cPHx2 fluorescence intensity
15
10
5
0
****
INPP4B(C842A)
INPP4B

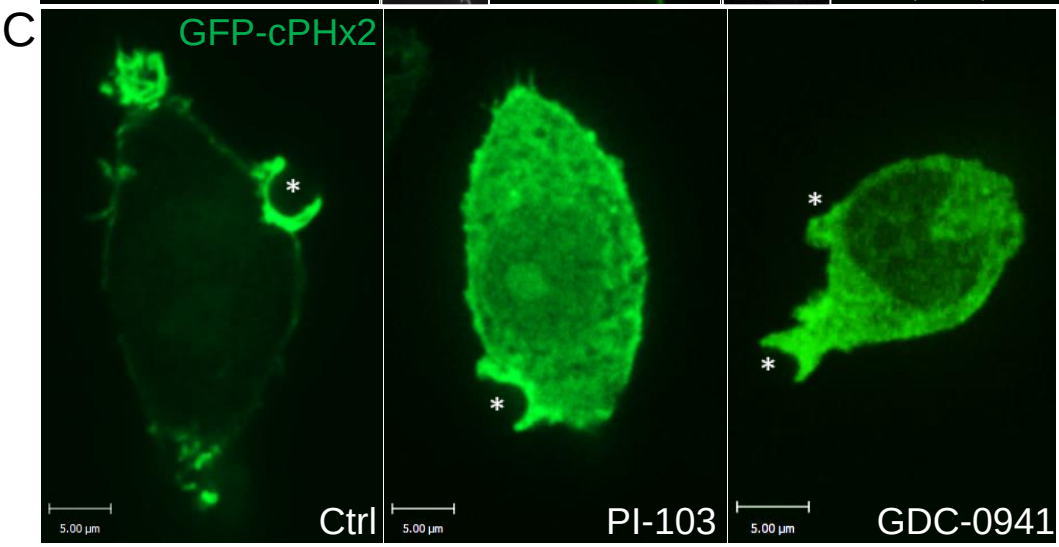
C
GFP-cPHx2
5.00 µm
Ctrl
PI-103
GDC-0941

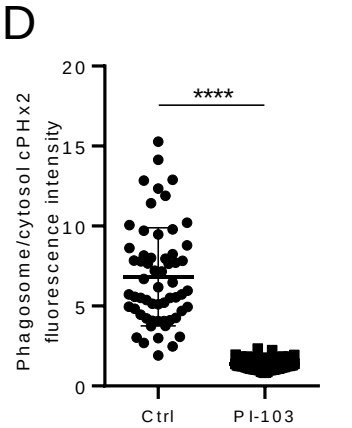
D
Phagosome/cytosol cPHx2 fluorescence intensity
20
15
10
5
0
****
Ctrl
PI-103

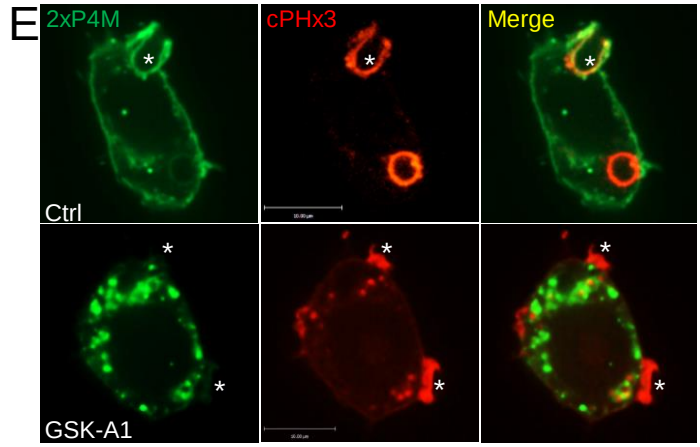
E
2xP4M
cPHx3
Merge
Ctrl
GSK-A1

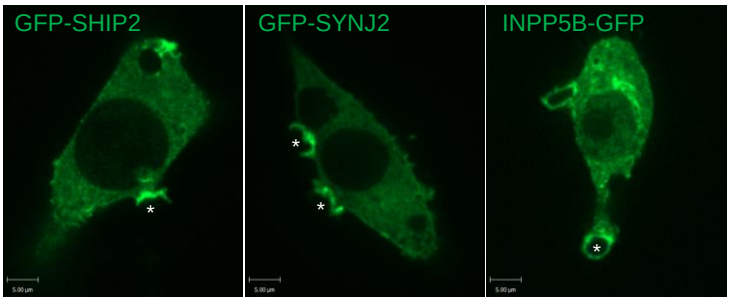
F
GFP-SHIP2
GFP-SYNJ2
INPP5B-GFP

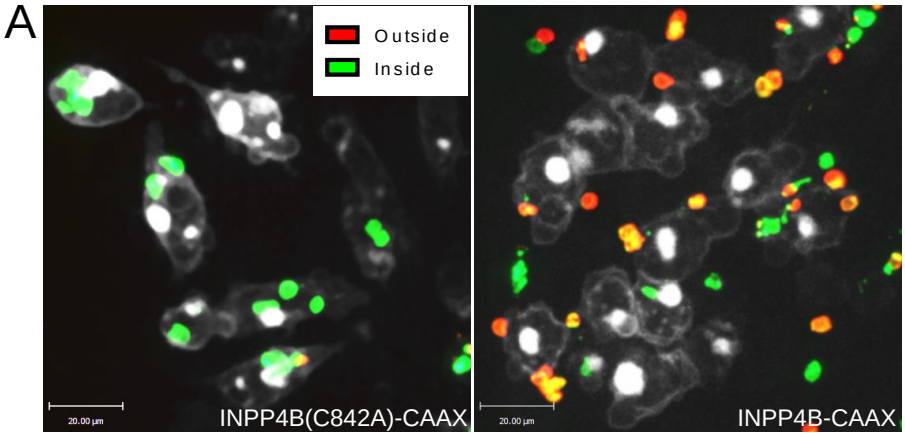
A
Outside
Inside
INPP4B(C842A)-CAAX
INPP4B-CAAX

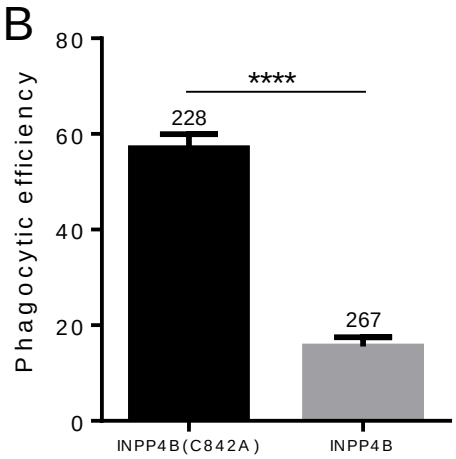
B
Phagocytic efficiency
80
60
40
20
0
****
228
267
INPP4B(C842A)
INPP4B

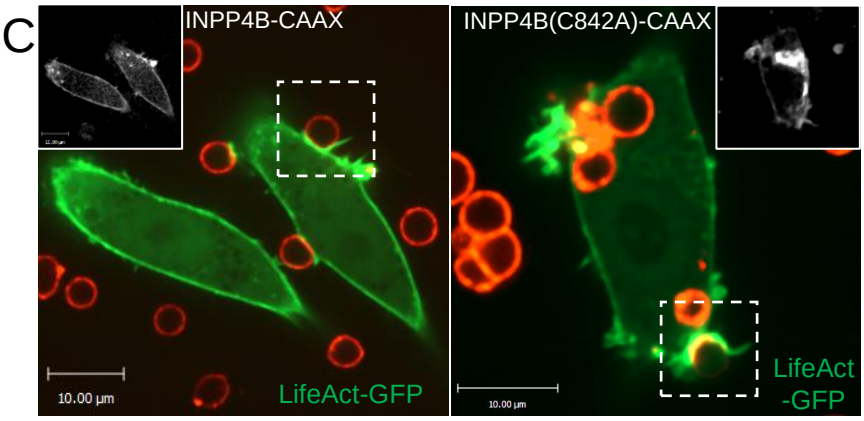
C
INPP4B-CAAX
INPP4B(C842A)-CAAX
10.00 µm
LifeAct-GFP
LifeAct
-GFP

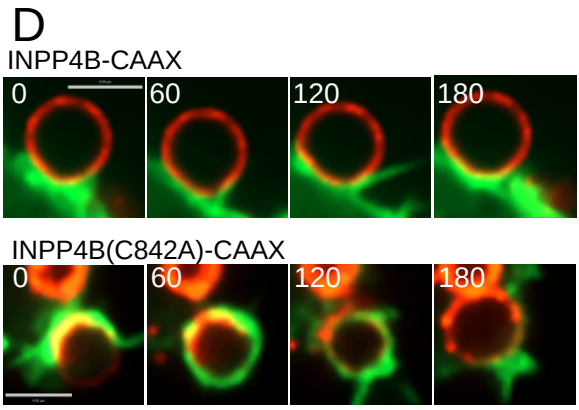
D
INPP4B-CAAX
0
60
120
180
INPP4B(C842A)-CAAX
0
60
120
180

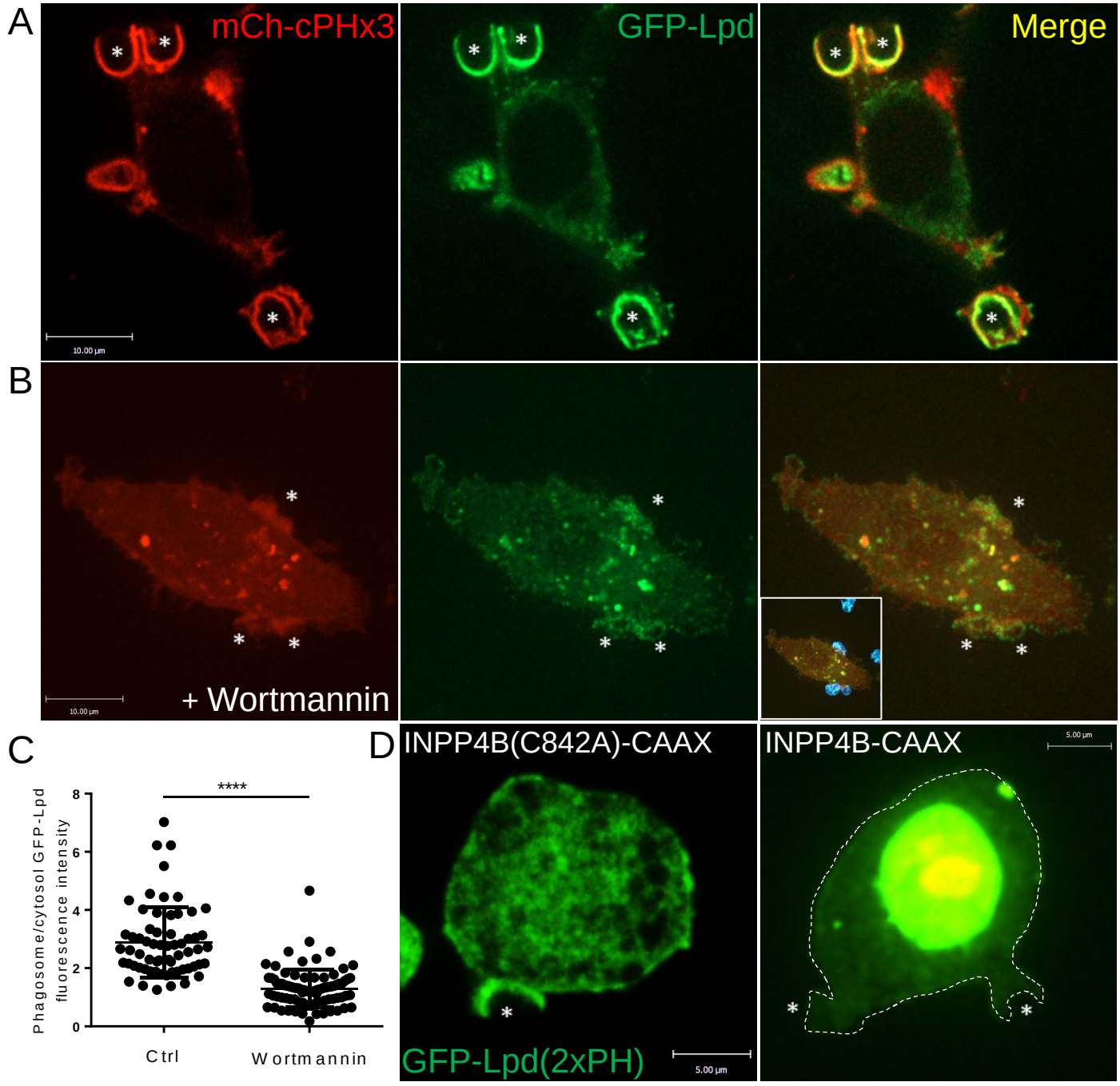
A
mCh-cPHx3
GFP-Lpd
Merge
10.00 µm
B
+ Wortmannin
10.00 µm
C
****
Phagosome/cytosol GFP-Lpd fluorescence intensity
8
6
4
2
0
Ctrl
Wortmannin
D
INPP4B(C842A)-CAAX
GFP-Lpd(2xPH)
5.00 µm
INPP4B-CAAX
5.00 µm

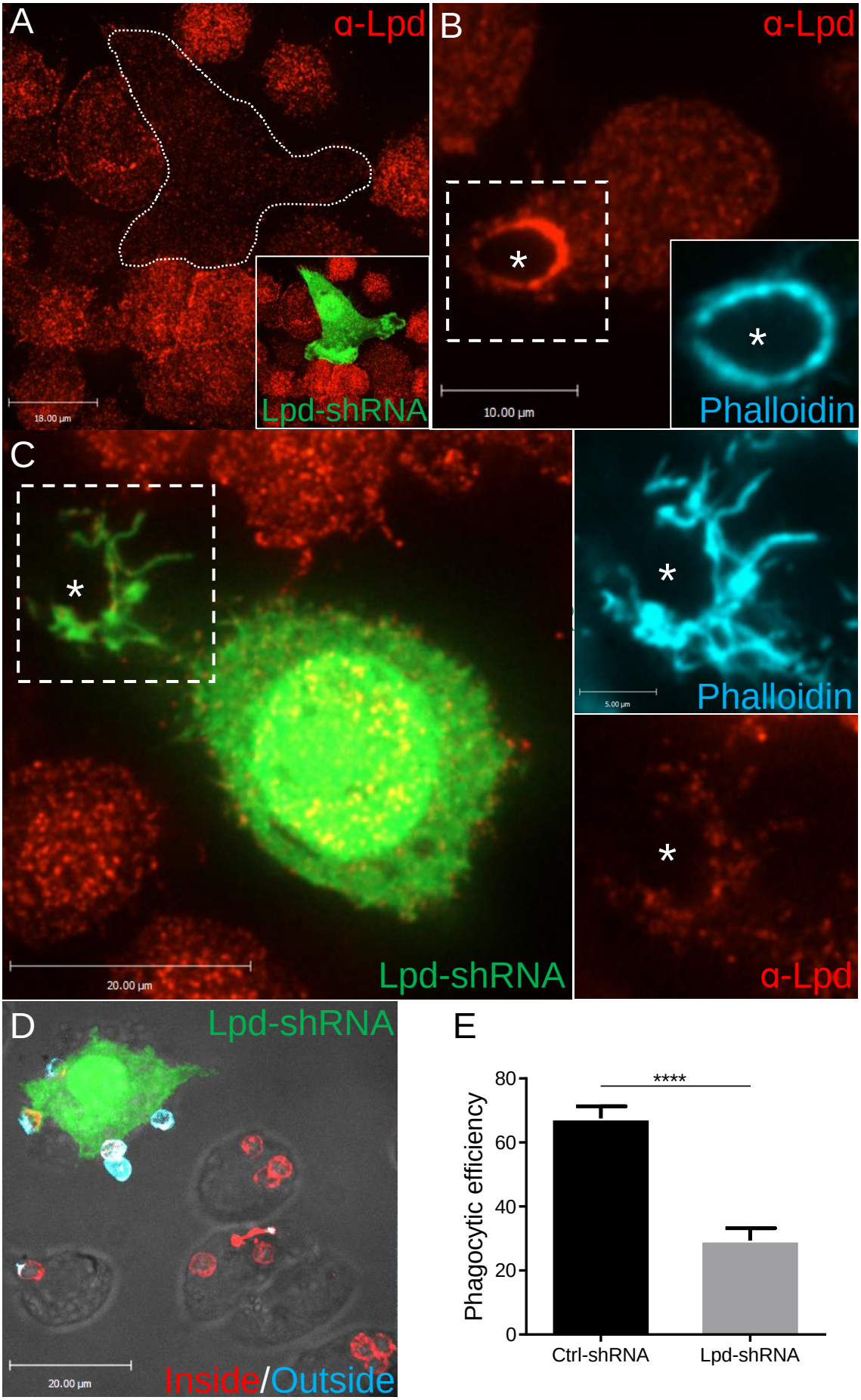
A
α-Lpd
Lpd-shRNA
18.00 µm
B
α-Lpd
*
10.00 µm
*
Phalloidin
C
*
20.00 µm
Lpd-shRNA
*
5.00 µm
Phalloidin
*
α-Lpd
D
Lpd-shRNA
20.00 µm
Inside/Outside
E
Phagocytic efficiency
80
60
40
20
0
****
Ctrl-shRNA
Lpd-shRNA

A

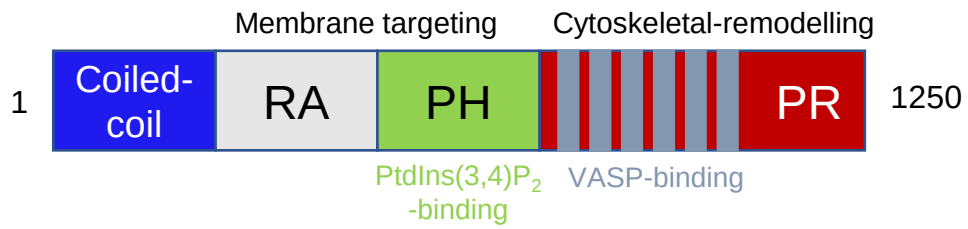
Membrane targeting
Cytoskeletal-remodelling
1
Coiled-coil
RA
PH
PR
1250
PtdIns(3,4)P2 -binding
VASP-binding

B

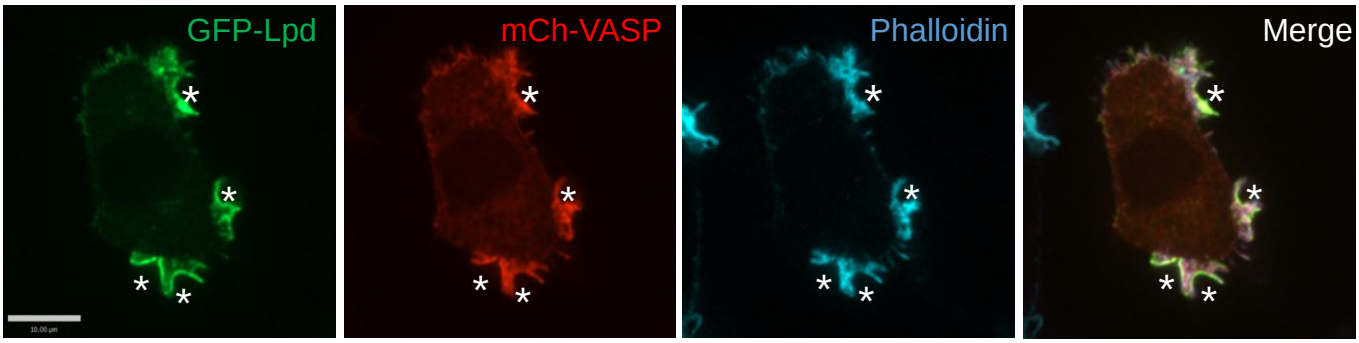
GFP-Lpd
mCh-VASP
Phalloidin
Merge

C

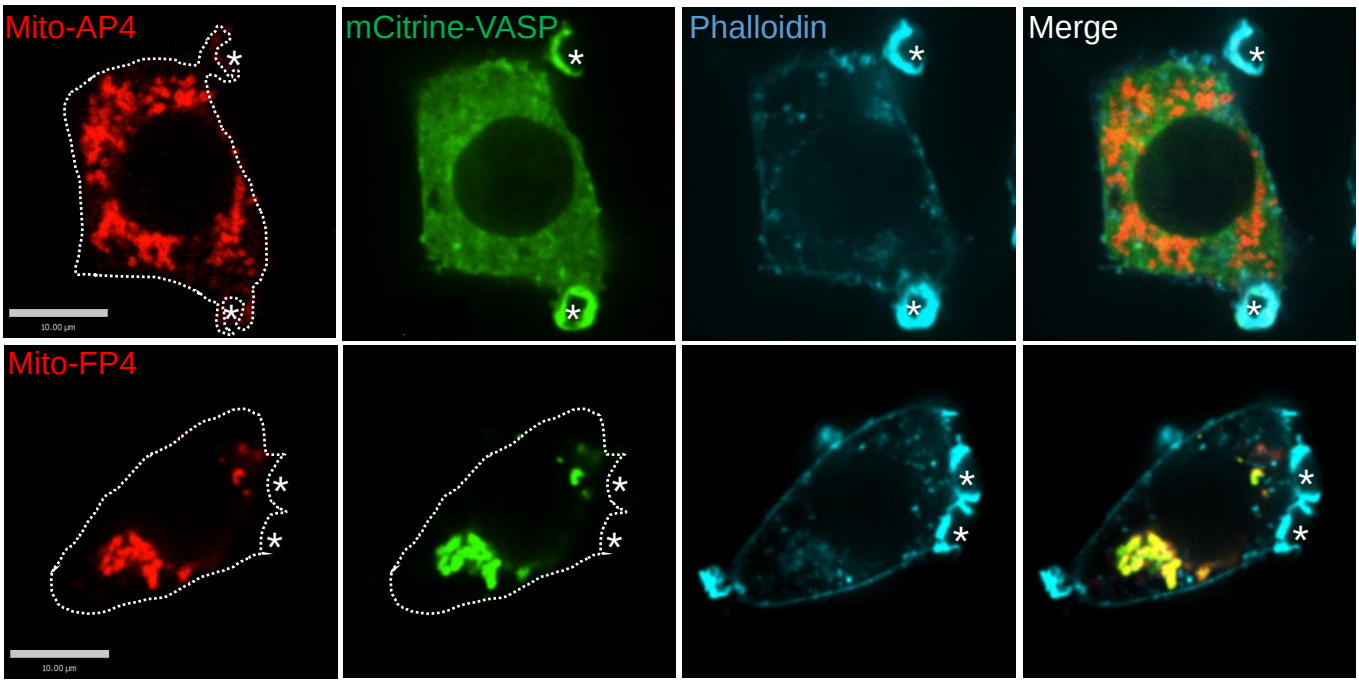
Mito-AP4
mCitrine-VASP
Phalloidin
Merge
Mito-FP4

D

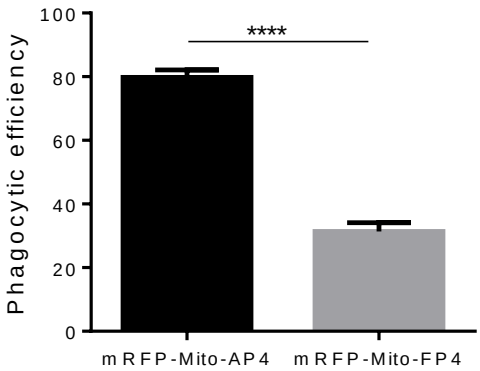
Phagocytic efficiency
100
80
60
40
20
0
****
mRFP-Mito-AP4
mRFP-Mito-FP4

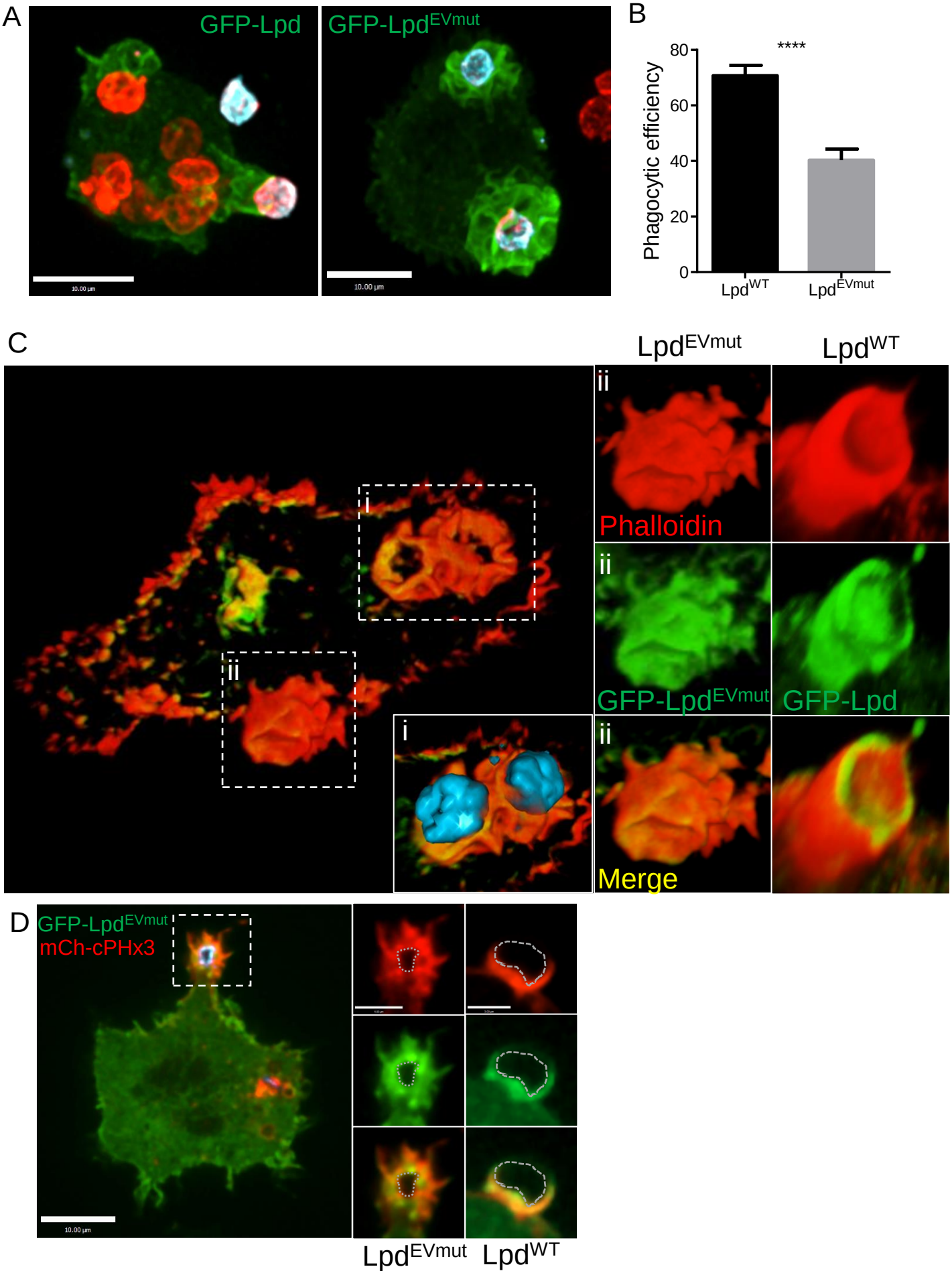
A
GFP-Lpd
GFP-Lpd^EVmut
10.00 µm
B
Phagocytic efficiency
80
60
40
20
0
****
Lpd^WT
Lpd^EVmut
C
Lpd^EVmut
Lpd^WT
i
ii
Phalloidin
GFP-Lpd^EVmut
GFP-Lpd
Merge
D
GFP-Lpd^EVmut
mCh-cPHx3
10.00 µm
Lpd^EVmut
Lpd^WT